Accelerated Multi-Objective Design of Miniaturized Microwave Components by Means of Nested Kriging Surrogates

Anna Pietrenko-Dabrowska[1] and Slawomir Koziel[2]

[1] Faculty of Electronics, Telecommunications and Informatics, Gdansk University of Technology, 80-233 Gdansk, Poland, anna.dabrowska@pg.edu.pl

[2] Engineering Optimization & Modeling Center, Reykjavik University, 101 Reykjavik, Iceland, koziel@ru.is,

Keywords: Microwave design, miniaturized components, multi-objective optimization, EM-driven design, surrogate modeling, nested kriging.

Abstract

Design of microwave components is an inherently multi-objective task. Often, the objectives are at least partially conflicting and the designer has to work out a suitable compromise. In practice, generating the best possible trade-off designs requires multi-objective optimization, which is a computationally demanding task. If the structure of interest is evaluated through full-wave electromagnetic (EM) analysis, the employment of widely used population-based metaheuristics algorithms may become prohibitive in computational terms. This is a common situation for miniaturized components, where considerable cross-coupling effects make traditional representations (e.g., network equivalents) grossly inaccurate. This paper presents a framework for accelerated EM-driven multi-objective design of compact microwave devices. It adopts a recently reported nested kriging methodology to identify the parameter space region containing the Pareto front and to render a fast surrogate, subsequently used to find the first approximation of the Pareto set. The final trade-off designs are produced in a separate, surrogate-assisted refinement process. Our approach is demonstrated using a three-section impedance matching transformer designed for the best matching and the minimum footprint area. The Pareto set is generated at the cost of only a few hundred of high-fidelity EM simulations of the transformer circuit despite a large number of geometry parameters involved.

1. Introduction

Miniaturization of microwave components has become an important design consideration due to the emergence of space-limited applications, including mobile communications [1,2], wearable/implantable devices [3,4], sensors [5], bio-medicine [6,7], body area networks [8,9], etc. Compact implementations of microwave circuits can be achieved in various ways; some of the popular techniques include utilization of high-permittivity substrates [10,11], transmission line (TL) folding [12], employing the slow-wave phenomenon [13,14], in particular, replacing conventional TLs by their shorter counterparts (e.g., compact microwave resonant cells, CMRCs) [15], [16], or multi-layer realizations (e.g., Low Temperature Cofired Ceramic, LTCC technology [17], [18]). Clearly, miniaturized circuits tend to feature complex topologies that normally have to be evaluated using full-wave electromagnetic (EM) analysis. This leads to practical problems when performing simulation-driven design tasks such as parametric optimization [19] or investigating the effects of manufacturing tolerances (e.g., statistical design [20]). Handling massive EM analyses in reasonable timeframes requires efficient numerical routines and many of these have been developed over the last two decades or so [21]-[27]. Some of available methods include surrogate-assisted routines (space mapping [21], response correction [22], feature-based optimization [23,24,25]), adjoint-based gradient algorithms [26], [27], or machine learning procedures [28], [29].

High-frequency design, just like almost any other task, is an inherently multi-objective endeavor [30], [31]. Typically, there are a few figures of interest that need to be accounted for at the same time, pertaining to both the electrical (impedance matching, power split ratio, bandwidth) and field properties (gain, sidelobe level for antenna arrays)

of the device, but also physical dimensions (e.g., footprint area) [32], [33]. Many of design objectives derived from the figures of interest are at least partially conflicting, i.e., an improvement of one generally leads to a degradation of the others. A representative example is a footprint area of planar microstrip circuits, a reduction of which normally stays in conflict with ensuring desired electrical performance [34]. Consequently, yielding a satisfactory design requires identification of a suitable trade-off between the design goals.

On a practical side, multi-objective design is often handled by reformulating the problem into a single-objective task [35]. The reason is strictly opportunistic: the abundance of single-objective optimization methods and their reliable implementations [36]-[38]. The mentioned reformulation can be realized either through objective aggregation (weighted sum methods [39], goal attainment method [40]) or by casting all but a primary goal into constraints [41]. The last approach is particularly attractive if the designer preferences are clearly articulated (e.g., footprint reduction while ensuring sufficient bandwidth specified through a hard acceptance threshold [42]).

On the other hand, genuine multi-objective optimization yields much more comprehensive information about the best possible design trade-offs. At the same time, it is more challenging. By far, the most popular solution techniques are population-based metaheuristics (genetic algorithms [43], particle swarm optimizers [44], differential evolution [45], firefly algorithm [46], and many others [47]-[49]), which are capable of rendering the entire Pareto set in a single algorithm run while retaining global search capabilities. Unfortunately, their computational complexity is tremendous so that they can normally be applied if the evaluation cost of the structure under design is not of

concern (e.g., an analytical or equivalent network model is utilized). If full-wave EM analysis is required, miniaturized microwave components being good examples, the employment of population-based methods may be prohibitive.

This paper discusses a novel approach to multi-objective design optimization of miniaturized components. Our methodology involves a recently reported nested kriging method [50], which is adopted for two purposes: (i) identification of the parameter space subset containing the Pareto-optimal designs (domain confinement), and (ii) construction of a fast surrogate model in that very region. Constraining the model domain allows for setting up a reliable model even if the number of design variables is relatively large, which is the major factor contributing to the computational efficiency of the method. The initial approximation of the Pareto set is generated with the aid of the surrogate. A separate refinement process is then applied to obtain the final set of the optimum trade-off designs. The presented approach is illustrated using a compact impedance matching transformer described by fifteen parameters. The Pareto set is obtained at the cost of only a few EM simulations of the circuit despite using a single-level (high-fidelity) EM model throughout the process. Benchmarking indicates that the supplementary surrogate model domain confinement through the nested kriging allows for reducing the optimization cost by almost seventy percent as compared to a state-of-the-art surrogate-assisted approach.

2. Multi-Objective Design Framework

This section outlines the multi-objective surrogate-assisted optimization framework, followed by the concept of surrogate domain confinement implemented through the nested kriging technique to reduce the computational cost of

model construction. The procedure of incorporating the nested kriging technique into the multi-objective design framework is also provided.

2.1. Surrogate-Assisted Multi-Objective Design

Multi-objective optimization (MO) aims at finding, within the considered parameter space, a set of globally non-dominated (or Pareto-optimal) designs [43], representing the best available trade-offs between the considered objectives, denoted as F_k, $k = 1, \ldots, N_{obj}$, with N_{obj} being the number of goals. Assuming minimization problems, the design featuring the objective vector $[F_1 \ \ldots \ F_{Nobj}]^T$ is said to be globally non-dominated if there is no other design featuring the objectives $[F'_1 \ \ldots \ F'_{Nobj}]^T$ such that $F'_k \leq F_k$ for all k and $F'_k < F_k$ for at least one k. The typical objectives for microwave components include, among others, device operating conditions or specifications concerning its electrical properties (e.g., center frequency, bandwidth, minimization of in-band reflection, achieving specific power split ratio) or material parameters (such as permittivity or thickness of the dielectric substrate, the component is implemented on).

The knowledge of available trade-offs is valuable because it allows for assessing suitability of a given structure in the context of a particular application, or to provide a conclusive comparison of alternative circuit solutions. Yet, EM-driven MO of microwave components may be impractical because of its considerable computational cost when using conventional methods, primarily, population-based metaheuristics [51]-[53]. Alternative means include utilization of fast replacement models (or surrogates) [54]-[55]. Undoubtedly, the most popular class of surrogates are data-driven models. The widely used techniques include kriging [56], Gaussian process regression [57], artificial neural networks (ANNs; [58]) or support vector regression (SVR; [59]).

Some of the recently proposed surrogate-assisted MO frameworks (e.g., [54],[60]-[61]) utilize the surrogate to yield the initial approximation of the Pareto set. To this end, the model is optimized directly using, e.g., a multi-objective evolutionary algorithm (MOEA; [62]). As the surrogate model is of a limited accuracy (often constructed at the level of coarse-mesh EM simulation model [63]), the initial Pareto-optimal designs $\boldsymbol{x}_s^{(k)}$, k = 1, …, N_{obj}, have to be fine-tuned in order to reach the accuracy of high-fidelity EM simulations. Let us denote by $\boldsymbol{R}(\boldsymbol{x})$ the computational model of the structure under design evaluated using EM analysis, where $\boldsymbol{x}$ denotes the adjustable parameter vector. In addition, $\boldsymbol{R}_s$ stands for the response of the surrogate. The refined Pareto designs $\boldsymbol{x}_f^{(k)}$ may be obtained through the following process

$$\boldsymbol{x}_f^{(k)} = \arg \min_{\substack{\boldsymbol{x},\ F_2(\boldsymbol{x}) \le F_2(\boldsymbol{x}_s^{(k)}) \\ \vdots \\ F_{N_{obj}}(\boldsymbol{x}) \le F_{Nobj}(\boldsymbol{x}_s^{(k)})}} F_1\left(\boldsymbol{R}_s(\boldsymbol{x}) + [\boldsymbol{R}(\boldsymbol{x}_s^{(k)}) - \boldsymbol{R}_s(\boldsymbol{x}_s^{(k)})]\right) \tag{1}$$

A perfect alignment between the surrogate $\boldsymbol{R}_s$ and the EM model at $\boldsymbol{x}_s^{(k)}$ is ensured by the correction term $\boldsymbol{R}(\boldsymbol{x}_s^{(k)}) - \boldsymbol{R}_s(\boldsymbol{x}_s^{(k)})$ [64].

Constructing the surrogate for MO purposes is not a trivial task. Due to the lack of prior knowledge about the location of the Pareto front within the parameter space, the model is supposed to cover broad parameter ranges. At the same time, the curse of dimensionality hinders the construction of surrogates in highly-dimensional spaces, frequently occurring for contemporary microwave components, especially miniaturized ones. Finally, the cost of training data acquisition is often prohibitive, even if yielding the model is numerically feasible.

A practical workaround is a confinement of the design space to the region containing the Pareto set, which can be arranged based on the single-objective optima

$\boldsymbol{x}^{*(k)} = \text{argmin}\{\boldsymbol{x} : F_k(\boldsymbol{R}(\boldsymbol{x}))\}$ [65]. The designs $\boldsymbol{x}^{*(k)}$ are the extreme Pareto-optimal designs that determine the span of the Pareto front. Using these, the lower and upper bounds for the design variables can be determined as $\boldsymbol{l}^* = \min\{\boldsymbol{x}^{*(1)},\ldots, \boldsymbol{x}^{*(N_{obj})}\}$ and $\boldsymbol{u}^* = \max\{\boldsymbol{x}^{*(1)},\ldots, \boldsymbol{x}^{*(N_{obj})}\}$ [64]. In most cases, the vast majority of the Pareto front is encompassed by the interval $[\boldsymbol{l}^*,\boldsymbol{u}^*]$. Another, more sophisticated method of establishing the Pareto front geometry is e.g., rotational space reduction [66], yet, its applicability is limited to two-objective problems.

Here, an enhanced surrogate-assisted MO procedure is introduced, which employs a recently reported nested kriging modelling [50] in order to reduce the design space more efficiently and to identify the allocation of the Pareto set. In the nested kriging, a data-driven model is constructed twice: the first model is utilized to identify the surrogate model domain, whereas the second one is the actual surrogate set up in that domain. Traditional modeling methods operate in interval-like domains, defined by the lower and upper parameter bounds. In practice, the designs optimal with respect to the chosen performance figures reside within small subsets of the such conventional domain, which is a result of complex interactions between design variables [67]. Hence, the surrogate model domain confinement with the nested kriging allows for achieving substantial cost savings. In the next section, we briefly recall the nested modeling concept, whereas its adaptation for MO purposes, which is a non-trivial task by itself, is explained in Section 2.4.

2.2. Surrogate Model Construction by Nested Kriging

In the nested kriging modeling, the figures of interest are denoted by f_k, $k = 1, \ldots, N$, and correspond to the MO design goals F_k of Section 2.1. The reference designs $\boldsymbol{x}^{(j)}$

$= [x_1^{(j)} \ldots x_n^{(j)}]^T$, $j = 1, \ldots, p$, optimized with respect to the performance vectors $\boldsymbol{F}^{(j)} = [F_1^{(j)} \ldots F_N^{(j)}]$, constitute the core of the nested kriging modeling. The vectors $\boldsymbol{F}^{(j)}$ are allocated within the objective space F the surrogate model is to cover [50]; F is delimited by the ranges $F_{k.\min} \le F_k^{(j)} \le F_{k.\max}$, $k = 1, \ldots, N$. In general, in order for the reference designs to provide the balanced information about the allocation of the optimum designs within the parameter space, they should be distributed as uniformly as possible within F. In the MO context, they need to include the extreme designs in order to account for the Pareto front geometry. If more detailed information is required, such as the Pareto front curvature, supplementary designs might also be needed. In practice, as the dimensionality of F is low, the typical number of the reference designs equals a dozen or so [50].

As stated above, in the nested kriging modeling procedure two surrogates are exploited. The first one, $\boldsymbol{s}_I(\boldsymbol{f})$, maps the objective space F into the design space X, i.e., it is a kriging interpolation [68] of the data set $\{\boldsymbol{f}^{(j)}, \boldsymbol{x}^{(j)}\}$ (pairs of the reference designs and the corresponding figures of interest; as shown in Fig. 1). The image $\boldsymbol{s}_I(F) \subset X$ of F through the first-level model $\boldsymbol{s}_I$, yields the initial approximation of the constrained surrogate domain. This means that $\boldsymbol{s}_I(F)$ represents the best information that is attainable from the reference points about the designs optimal with respect to all $\boldsymbol{f} \in F$. Nevertheless, as this information is approximate, $\boldsymbol{s}_I(F)$ has to be expanded. To this end, an orthogonal extension towards the normal vectors of $\boldsymbol{s}_I(F)$ is performed. The goal is to ensure that all optimum designs are included in the domain. Let us denote the normal vectors at $\boldsymbol{f}$ as $\boldsymbol{v}_n^{(k)}(\boldsymbol{f})$, $k = 1, \ldots, n - N$ [50]. In addition, let us define: $\boldsymbol{x}_{\max} = \max\{\boldsymbol{x}^{(k)}, k = 1, \ldots, p\}$, $\boldsymbol{x}_{\min} = \min\{\boldsymbol{x}^{(k)}, k = 1, \ldots, p\}$, $\boldsymbol{x}_d = \boldsymbol{x}_{\max} - \boldsymbol{x}_{\min}$. Then, the extension coefficients are defined as follows

$$\boldsymbol{\alpha}(\boldsymbol{f}) = [\alpha_1(\boldsymbol{f}) \ldots \alpha_{n-N}(\boldsymbol{f})]^T = \frac{D}{2}\left[| \boldsymbol{x}_d \boldsymbol{v}_n^{(1)}(\boldsymbol{f}) | \ \ldots \ | \boldsymbol{x}_d \boldsymbol{v}_n^{(n-N)}(\boldsymbol{f}) | \right]^T \tag{2}$$

In (2), D denotes a user-defined thickness parameter determining the amount of the orthogonal extension [50]. Having α_k, the surrogate model domain X_S can be defined. It resides between the manifolds M_+ and M_- (see Fig. 1(b))

$$M_{\pm} = \left\{ \boldsymbol{x} \in X : \boldsymbol{x} = \boldsymbol{s}_I(\boldsymbol{f}) \pm \sum_{k=1}^{n-N} \alpha_k(\boldsymbol{f}) \boldsymbol{v}_n^{(k)}(\boldsymbol{f}) \right\} \tag{3}$$

The formal definition of X_S is as follows

$$X_S = \left\{ \begin{array}{c} \boldsymbol{x} = \boldsymbol{s}_I(\boldsymbol{f}) + \sum_{k=1}^{n-N} \lambda_k \alpha_k(\boldsymbol{f}) \boldsymbol{v}_n^{(k)}(\boldsymbol{f}) : \boldsymbol{f} \in F, \\ -1 \le \lambda_k \le 1, k = 1, \ldots, n-N \end{array} \right\} \tag{4}$$

The second kriging surrogate is constructed in X_S using $\{\boldsymbol{x}_B^{(k)}, \boldsymbol{R}(\boldsymbol{x}_B^{(k)})\}_{k = 1, \ldots, N_B}$, as the training data set. Some noteworthy advantages of defining X_S as in (4) should be pointed out, i.e., a straightforward arrangement of a uniform sampling (important for yielding reliable model) and convenient model optimization (fundamental for design applications). For the sake of brevity, only the essential aspects of the nested kriging modeling framework have been recalled here; more details can be found in [50].

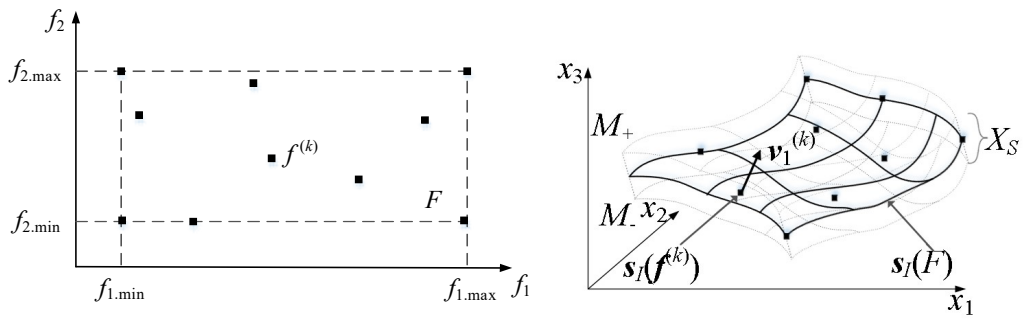

Fig. 1. Graphical illustration of the nested kriging modeling concept (shown for two-dimensional objective space and three dimensional parameter space): (a) reference designs and objective space F; (b) the image $\boldsymbol{s}_I(F)$ of the first-level surrogate model and the normal vector $\boldsymbol{v}_1^{(k)}$ at $\boldsymbol{f}^{(k)}$; the manifolds M_- and M_+ delineating the surrogate model domain X_S being the orthogonal extension of $\boldsymbol{s}_I(F)$.

2.3. Nested Kriging for Multi-Objective Design Framework

In this section, utilization of the nested kriging modeling for MO purposes is outlined. Here, the primary challenge is that the objective space is merely a small part of an interval, e.g., for $N_{obj} = 2$ it is a one-dimensional object (curve), whereas for $N_{obj} = 3$ it is a part of a 2D surface. In the nested kriging MO, the figures of interest f_k of the nested surrogate and the MO design objectives F_k, are identical, i.e., $N = N_{obj}$. In single-objective nested kriging, a uniform distribution of the reference designs within the interval-like objective space F was required. In the MO context, they need to represent the Pareto front geometry, i.e., include the extreme designs $\boldsymbol{x}^{*(k)} = \text{argmin}\{\boldsymbol{x} : F_k(\boldsymbol{R}(\boldsymbol{x}))\}$, and, if needed, a certain number of additional designs for describing the front curvature. The reference designs may be obtained by solving

$$\boldsymbol{x}(\boldsymbol{w}) = \arg\min_{\boldsymbol{x}} F_1\left(\boldsymbol{R}(\boldsymbol{x})\right) \tag{5}$$

subject to constraints

$$F_j(\boldsymbol{x}) \le \sum_{l=1}^{N} w_l F_j(\boldsymbol{x}^{*(l)}), \qquad j = 2,...,N \tag{6}$$

where $\boldsymbol{w} = [w_1 \ \ldots \ w_N]^T$ refers to the vector of weights being a convex combination, i.e.,

$$0 \le w_j \le 1 \quad \text{and} \quad \sum_{j=1}^{N} w_j = 1 \tag{7}$$

The vectors of weights for the extreme Pareto-optimal designs $\boldsymbol{x}^{*(k)}$ are as follows: $\boldsymbol{w} = [0 \ \ldots \ 1 \ \ldots \ 0]^T$ with 1 on the kth position. In order to distribute the reference designs along the Pareto front, other arrangements should be included, e.g., $\boldsymbol{w} = [1/N \ 1/N \ \ldots \ 1/N]^{\mathrm{T}}$ that refers to the front center.

For the sake of convenience, a mapping between the weighting vectors $\boldsymbol{w}$ (in particular those fulfilling the condition (7)) and the segment of the objective space

corresponding to the Pareto front should be established. First, let us define an auxiliary transformation from a unit N–1 simplex S^{N-1} onto the space of the weights $\boldsymbol{w}$

$$h_0(\boldsymbol{z}) = \begin{bmatrix} 1 \\ 0 \\ \vdots \\ 0 \end{bmatrix} + \begin{bmatrix} -1 & -1 & \cdots & -1 \\ 1 & 0 & \cdots & 0 \\ 0 & 1 & \cdots & 0 \\ \vdots & \vdots & \ddots & \vdots \\ 0 & 0 & \cdots & 1 \end{bmatrix} \cdot \boldsymbol{z} \tag{8}$$

The above transformation facilitates building the surrogate model and allocation of the training data. The unit simplex S^{N-1} is described as follows

$$S^{N-1} = \left\{ \boldsymbol{z} = [z_1 \ldots z_{N-1}]^T : 0 \le z_k \le 1 \text{ and } \sum_{k=1}^{N-1} z_k \le 1 \right\} \tag{9}$$

Graphical illustration of adopting the nested kriging for the two- and three-objective cases MO is shown in Fig. 2. The objective vectors $\boldsymbol{F}(\boldsymbol{w})$ correspond to the selected reference designs $\boldsymbol{x}(\boldsymbol{w})$, whereas $\boldsymbol{F}_k = [F_1(\boldsymbol{x}^{*(k)}) \ \ldots \ F_N(\boldsymbol{x}^{*(k)})]^T$, k = 1, …, N, refer to the extreme Pareto designs. Clearly, the reference designs, the number of which is normally small, only provide a rough description of the Pareto front geometry, thus, some extension of the region where they reside is required. Therefore, it is the extended region O, defined as the set of all points of the form

$$\boldsymbol{w} = h_0(\boldsymbol{z}) \cdot (1 + d) \quad \text{with} \quad \boldsymbol{z} \in S^{N-1} \quad \text{and} \quad -d_w \le d \le d_w \tag{10}$$

that constitutes the actual domain of the first-level surrogate; with d_w being the extension factor (in this work d_w = 0.05).

The reference designs serve to construct the first-level surrogate for MO, which is a merger of two transformations. The first one is the mapping from the Cartesian product of $S^{N-1} \times [-d_w, d_w]$ onto the extended objective space region O, whereas the second is the "conventional" first-level model $\boldsymbol{s}_I$ from O into X (see Section 2.2). It should be noted, that

the sole purpose of introducing the former transformation is to facilitate uniform data sampling, as it is easier to acquire data on $S^{N-1} \times [-d_w, d_w]$ than directly within O. Next, the second-level surrogate is built in the domain defined similarly as in basic nested kriging modeling of Section 2.2, yet, an orthogonal extension of $\boldsymbol{s}_l(O)$, instead of $\boldsymbol{s}_l(F)$, is carried out. It should be reiterated that accurate identification of the Pareto front is possible due to the employment of the nested modeling technique for MO described in this section.

As far as the number of the reference designs is concerned, it should provide a valid Pareto front representation, e.g., for $N_{obj} = 2$, a reasonable number of the reference designs seems to be up to three or four (cf. Fig. 2(a)), whereas for $N_{obj} = 3$, up to six or seven should suffice (cf. Fig. 2(b)). The acquisition of the reference designs certainly induces unavoidable computational expenses. Yet, in the presented framework, the cost of finding extra reference designs, other than the extreme ones, is low as good initial points for seeking $\boldsymbol{x}(\boldsymbol{w})$ may simply be obtained as

$$\boldsymbol{x}\left(\boldsymbol{w}\left(0\right)\right) = \sum_{l=1}^{N} w_l \boldsymbol{x}^{*(l)} \tag{11}$$

In (11), $\boldsymbol{x}^{*(l)}$, $l = 1, \ldots, N$, refer to the extreme, single-objective designs corresponding to $\boldsymbol{w} = [0 \ldots 1 \ldots 0]^T$ with 1 on the lth position.

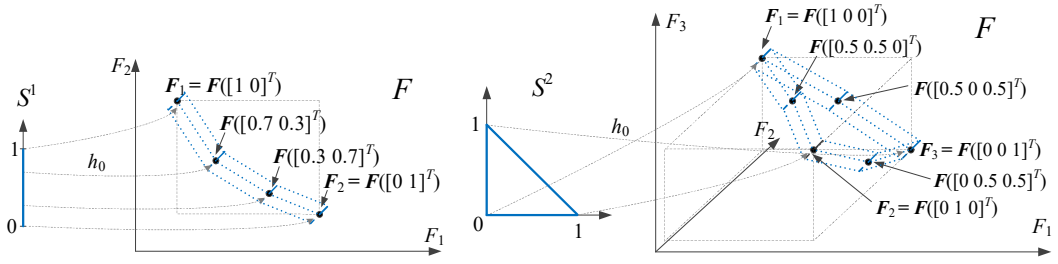

Fig. 2. Adaptation of the nested kriging technique for MO purposes: the objective space F and the objective vectors $\boldsymbol{F}$ corresponding to the selected reference designs. The objective space regions, where the nested kriging model is to be set up, are marked using dotted lines. The mapping h_0 from the unity simplex onto the objective space region is also shown: (a) two-objective case, (b) three-objective case.

Figure 3 summarizes the nested surrogate modeling process for MO. The second-level model is optimized using MOEA and yields the initial Pareto set, which needs to be further refined using (1) (cf. Section 2.1). In this work, for the sake of demonstration of the computational efficiency of the proposed methodology, only high-fidelity EM simulations are utilized. The surrogate itself is optimized in the original domain of the first-level surrogate, i.e., $S^{N-1} \times [-d_w, d_w]$. In order to evaluate the device response, the designs $\boldsymbol{y} \in S^{N-1} \times [-d_w, d_w]$ are converted into the weight vectors $\boldsymbol{w}$ using (10). Subsequently, the first-level model $\boldsymbol{s}_I$ is used to transform them into the designs $\boldsymbol{x} \in X$ from the parameter space.

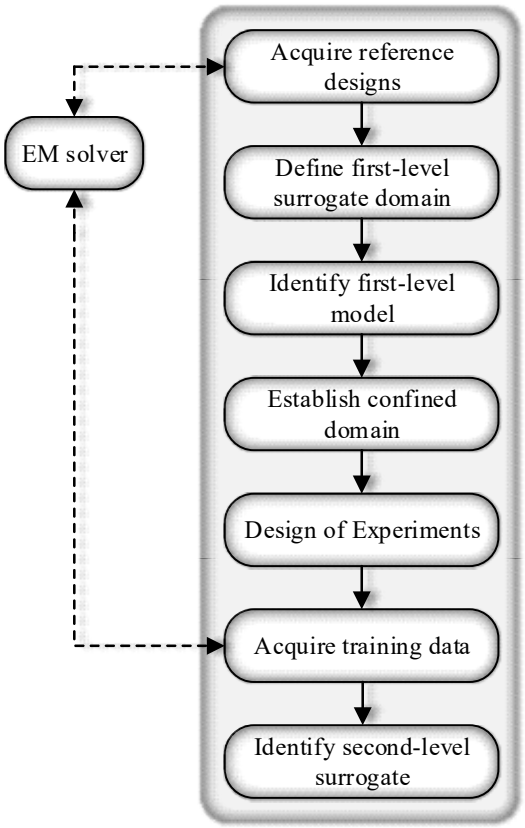

Fig. 3. The nested surrogate modeling process for multi-objective optimization: a flowchart.

The advantage of the presented approach is that it makes it possible to operate within a geometrically simple domain delineated by the lower/upper bounds $0 \le y_k \le 1$, $k = 1, \ldots, N-1$, $-d_w \le y_N \le d_w$, with a linear constraint $\sum_{k=1,\ldots,N-1} y_k \le 1$, regardless of the actual shape of the Pareto front. The flowchart of Fig. 4 summarizes the process of surrogate model evaluation.

3. Numerical Validation

The methodology proposed in this paper is illustrated with a CMRC-based three-section transformer described using fifteen geometry parameters and designed to simultaneously minimize the in-band reflection and the footprint area. The framework is benchmarked against surrogate-assisted MO procedure of Section 2.1.

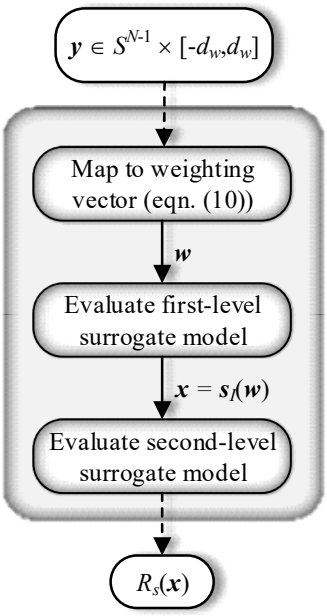

Fig. 4. Flow diagram of the evaluation of the nested kriging surrogate for MO process. The model is operated from the domain $S^{N-1} \times [-d_w, d_w]$, next the argument $\boldsymbol{y}$ is mapped into the space of the weighting vectors using (10) and then into the surrogate model domain X_S. The second-level surrogate is finally evaluated within X_S and produces the responses of the structure under design.

A remark should be made, that only high-fidelity EM simulations are used for the verification purposes. Hence, it is not possible to compare the obtained results directly to those yielded by variable-fidelity frameworks. Notwithstanding, the proposed technique can be expanded to the variable-fidelity setup in a straightforward manner.

3.1. Case Study: Impedance Matching Transformer

Our demonstration example is the 50-to-100 Ohm impedance matching transformer shown in Fig. 5(b) [69]. The device utilizes a compact microstrip resonant cell (CMRC) introduced in order to shorten the entire structure (see Fig. 5(a)). The design variables are $\boldsymbol{x} = [l_{1.1}\ l_{1.2}\ w_{1.1}\ w_{1.2}\ w_{1.0}\ l_{2.1}\ l_{2.2}\ w_{2.1}\ w_{2.2}\ w_{2.0}\ l_{3.1}\ l_{3.2}\ w_{3.1}\ w_{3.2}\ w_{3.0}]^T$. The transformer is implemented on RF-35 substrate ($\varepsilon_r = 3.5$, $h = 0.762$ mm, $\tan\delta = 0.0018$). The device operating range is 1.75 GHz to 4.25 GHz. Two figures of interest are considered: (i) minimization of the in-band reflection (F_1), and (ii) minimization of the footprint area (F_2). The computational model $\boldsymbol{R}$ is simulated in CST Microwave Studio (~280,000 mesh cells, simulation time 2.5 min).

3.2. Experimental Setup and Results

Four reference designs are utilized: the first two corresponding to the two extreme designs, and the two supplementary designs corresponding to $z = 0.33$ and $z = 0.66$ (cf. (8)).

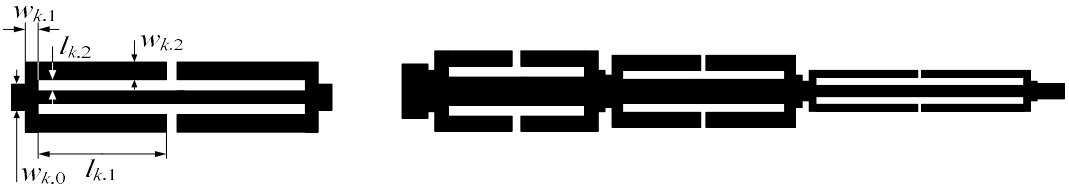

(a) (b)

Fig. 5. CMRC-based three-section impedance matching transformer used for verification purposes: (a) compact microstrip resonant cell (CMRC) cell, (b) transformer geometry.

The adopted value of the thickness parameter, $D = 0.05$, ensures good predictive power of the surrogate; at the same time, a small number of training data points is required. For the comprehensive discussion of the relationship between the modeling error and the value of parameter D see [50].

The nested kriging surrogate for MO purposes was constructed using only 200 data samples, according to the methodology of Section 2.4. The relative RMS error, defined as $||\boldsymbol{R}(\boldsymbol{x}) - \boldsymbol{R}_s(\boldsymbol{x})||/||\boldsymbol{R}(\boldsymbol{x})||$, is 4.1%. For benchmarking, the surrogate was also set up within the space reduced in a crude manner, i.e., the interval $\boldsymbol{l}^* = \min\{\boldsymbol{x}^{*(1)}, \boldsymbol{x}^{*(2)}\}$ and $\boldsymbol{u}^* = \max\{\boldsymbol{x}^{*(1)}, \boldsymbol{x}^{*(2)}\}$. In practice, the interval defined this way encompasses vast majority of the Pareto front [55]. Although the surrogate was set up with 1600 training samples, the observed model error is as high as 10.4%. Clearly, this comparison demonstrates the benefits of adopting the proposed approach.

The first approximation of the Pareto set was yielded by MOEA algorithm [69] (see Fig. 6). The selected EM-simulated Pareto-optimal designs, before and after the refinement process are also shown in Fig. 6. The corresponding numerical data has been gathered in Table I. The reflection characteristics of the transformer for the selected designs are presented in Fig. 7. Table II provides the breakdown of the optimization cost.

3.3. Benchmarking and Discussion

In the proposed framework, the cost of the training data acquisition for constructing the surrogate model, being the main contributor to the total optimization overhead, is reduced in a significant manner (from 1600 to merely 200 samples). Hence, the overall expenses are reduced by around 65 percent. In addition, regardless of using solely single-fidelity models, the overall MO cost is as low as 745 EM simulations. These

savings have been obtained as a consequence of setting up the surrogate model in a considerably smaller domain, rendered with the use of the nested kriging technique. At the same time, the cost reduction is accompanied by a significantly better predictive power of the surrogate. It should be noted that, from the standpoint of surrogate model construction, the presented case is a challenging one because of the parameter space dimensionality (fifteen variables) and broad parameter ranges.

Table I CMRC-based Transformer: Pareto-Optimal Designs

		Pareto-optimal design									
		$\boldsymbol{x}^{(1)}$	$\boldsymbol{x}^{(2)}$	$\boldsymbol{x}^{(3)}$	$\boldsymbol{x}^{(4)}$	$\boldsymbol{x}^{(5)}$	$\boldsymbol{x}^{(6)}$	$\boldsymbol{x}^{(7)}$	$\boldsymbol{x}^{(8)}$	$\boldsymbol{x}^{(9)}$	$\boldsymbol{x}^{(10)}$
Objectives	F_1 [dB]	–26.8	–26.5	–25.2	–24.4	–23.3	–22.6	–21.8	–21.2	–20.3	–19.8
	F_2 [mm^2]	71.4	62.3	57.1	51.1	46.2	41.8	37.6	35.4	33.4	31.9
Geometry parameters [mm]	$l_{1.1}$	3.74	3.82	3.67	3.31	2.93	2.65	2.50	2.63	2.91	3.40
	$l_{1.2}$	0.28	0.26	0.24	0.21	0.19	0.17	0.15	0.14	0.14	0.15
	$w_{1.1}$	0.77	0.78	0.79	0.79	0.80	0.80	0.80	0.80	0.80	0.80
	$w_{1.2}$	0.52	0.44	0.40	0.38	0.37	0.35	0.32	0.27	0.23	0.16
	$w_{1.0}$	0.30	0.30	0.31	0.34	0.35	0.37	0.37	0.38	0.36	0.34
	$l_{2.1}$	4.30	3.97	3.80	3.51	3.31	3.14	2.88	2.71	2.63	2.55
	$l_{2.2}$	0.28	0.26	0.25	0.23	0.21	0.20	0.18	0.17	0.15	0.14
	$w_{2.1}$	0.49	0.43	0.39	0.36	0.34	0.33	0.30	0.29	0.24	0.19
	$w_{2.2}$	0.25	0.30	0.32	0.41	0.47	0.51	0.54	0.52	0.50	0.47
	$w_{2.0}$	1.64	1.71	1.71	1.74	1.76	1.74	1.70	1.66	1.54	1.42
	$l_{3.1}$	4.55	4.37	4.14	3.85	3.54	3.31	3.12	3.02	2.99	3.12
	$l_{3.2}$	0.19	0.14	0.16	0.25	0.35	0.43	0.49	0.45	0.37	0.25
	$w_{3.1}$	0.29	0.26	0.26	0.24	023	0.21	0.21	0.20	0.19	0.20
	$w_{3.2}$	0.25	0.27	0.26	0.27	0.27	0.27	0.27	0.28	0.28	0.29
	$w_{3.0}$	0.58	0.70	0.72	0.78	0.86	0.92	1.02	1.19	1.31	1.42

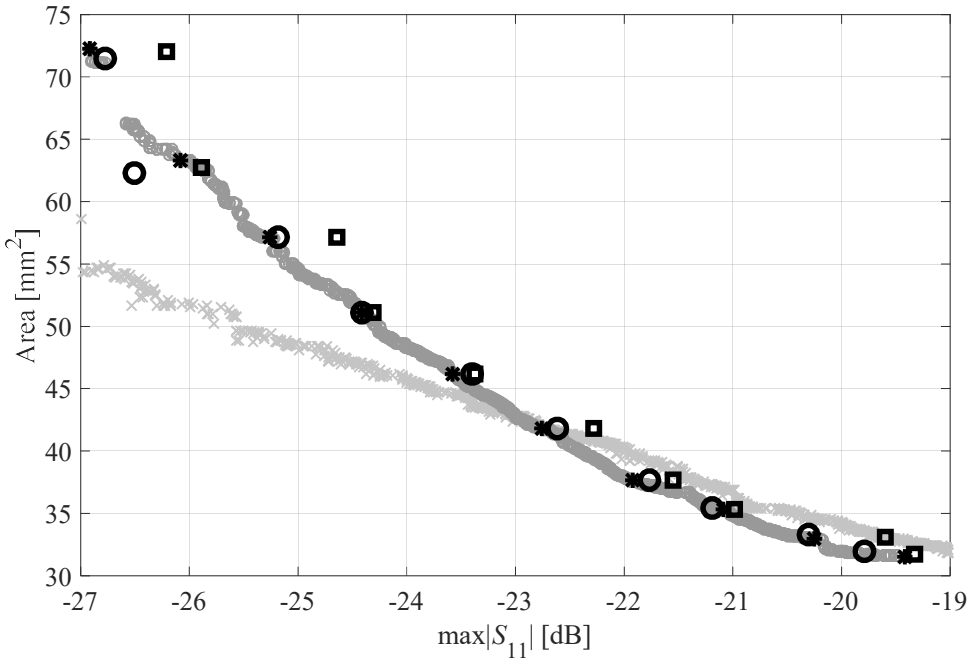

Fig. 6. Pareto-optimal solutions found for CMRC-based three-section transformer: (o) initial set obtained with MOEA, (*) selected designs for refinement, (□) EM-simulated selected designs, (O) EM-simulated refined designs.

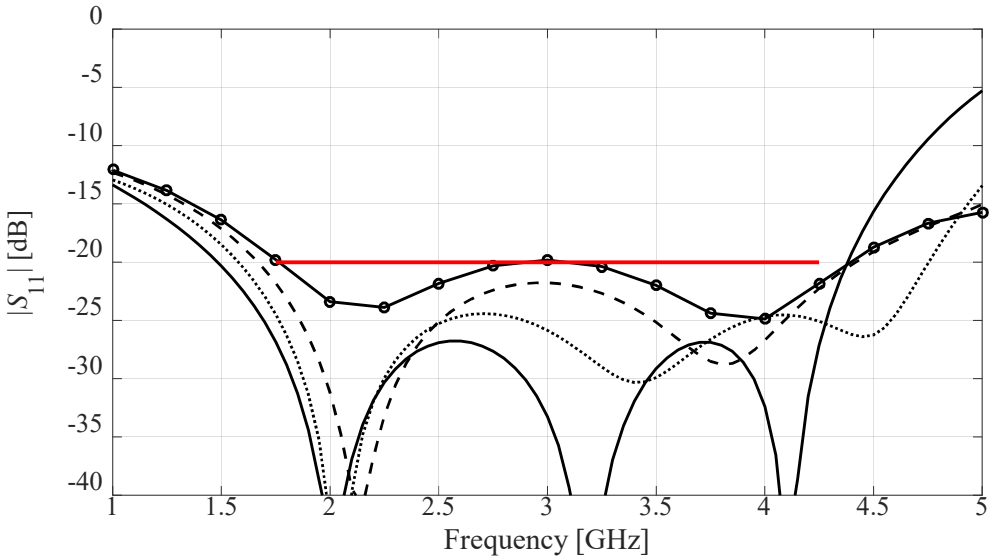

Fig. 7. Reflection characteristics of the transformer for the selected Pareto-optimal designs of Table I: $\boldsymbol{x}^{(1)}$ (—), $\boldsymbol{x}^{(4)}$ (····), $\boldsymbol{x}^{(7)}$ (- - -), and $\boldsymbol{x}^{(10)}$ (-o-).

Table II Optimization Cost Breakdown

Cost item	Surrogate model domain	
	X_S (this work)	Hypercube [$\boldsymbol{l}^*$,$\boldsymbol{u}^*$]
Extreme points	515 × $\boldsymbol{R}$	515 × $\boldsymbol{R}$
Data acquisition for kriging surrogate	200 × $\boldsymbol{R}$	1600 × $\boldsymbol{R}$
MOEA optimization*	N/A	N/A
Refinement	30 × $\boldsymbol{R}$	30 × $\boldsymbol{R}$
Total cost#	745 × $\boldsymbol{R}$ (31 h)	2145 × $\boldsymbol{R}$ (89 h)

* The cost of MOEA optimization is negligible compared to other stages of the process.
# The total cost (equivalent number of EM simulations; CPU time shown in brackets).

4. Conclusion

In the paper, a robust technique for multi-objective design optimization of microwave structures has been presented. The framework exploits a nested kriging modeling approach for the two purposes: (i) identification of the region of the design space where the best trade-off designs reside, and (ii) constructing, within that region, a fast surrogate model that delivers an initial approximation of the Pareto set. In this work, the nested kriging framework has been generalized to handle an arbitrary subset of the objective space rather than the interval, as in the original rendition of the technique.

The surrogate-assisted MO framework has been validated using the three-section transformer, optimized for two objectives. The reduction of the computational cost of around 65 percent has been obtained in comparison to the benchmark surrogate-assisted approach. At the same time, the quality of the Pareto front representation has been improved.

Acknowledgement

The authors would like to thank Dassault Systemes, France, for making CST Microwave Studio available. This work is partially supported by the Icelandic Centre for Research (RANNIS) Grant 174114051 and by National Science Centre of Poland Grant 2018/31/B/ST7/02369.

References

[1] Mohamed HAE, El-Shaarawy HB, Abdallah EA, El-Hennawy HMS. A very compact novel multi-band BPF for recent mobile/satellite communication systems. *Progr Electromagn Research C*. 2014;50:47-56.

[2] Sun L, Feng H, Li Y, Zhang Z. Compact 5G MIMO mobile phone antennas with tightly arranged orthogonal-mode pairs. *IEEE Trans Antennas Propag.* 2018;66(11);6364-6369.

[3] Biswas AK, Chakraborty U. A compact wide band textile MIMO antenna with very low mutual coupling for wearable applications. *Int J RF Microw Comput Aided Eng*. 2019;29:e21769.

[4] Shon A, Chu JU, Jung J, Kim H, Youn I. An implantable wireless neural interface system for simultaneous recording and stimulation of peripheral nerve with a single cuff electrode. *Sensors*. 2018;18(1):1-26.

[5] Hamzah H, Abduljabar A, Lees J, Porch A. A compact microwave microfluidic sensor using a re-entrant cavity. *Sensors*. 2018;18(3):910.

[6] Yang L, Zhou YJ, Zhang C, Yang XM, Yang X, Tan C. Compact multiband wireless energy harvesting based battery-free body area networks sensor for mobile healthcare. *IEEE J Electromagn RF Microw Medicine Biology*. 2018;2(2):109-115.

[7] Zhang H, Chen X, Li M, Yang F, Xu S. A compact dual-band folded-cavity antenna for microwave biomedical imaging applications. *IEEE Int Conf Comput Electromagn (ICCEM)*, Shanghai, China, 2019:1-3.

[8] Mohamed M, Cheffena M, Moldsvor A, Fontan FP. Physical statistical channel model for off-body area network. *IEEE Antennas Wireless Propag Lett*. 2017;16:1516-1519.

[9] Wagih M, Wei Y, Beeby S. Flexible 2.4 GHz node for body area networks with a compact high-gain planar antenna. *IEEE Antennas Wireless Propag Lett*. 2019;18(1):49-53.

[10] Sarkhel A, Mitra D, Bhadra Chaudhuri SR. A compact metamaterial with multi-band negative-index characteristics. *Appl Phys: A*. 2016;122(4):471.

[11] Shaw T, Mitra D. Wireless power transfer system based on magnetic dipole coupling with high permittivity metamaterials. *IEEE Antennas Wireless Propag Lett*. 2019;18(9):1823-1827.

[12] Letavin D. Miniature microstrip branch line coupler with folded artificial transmission lines. *Int J Electron Commun*. 2019;99:pp. 8-13.

[13] Coromina J, Vélez P, Bonache J, Aznar-Ballesta F, Fernández-Prieto A, Martín F. Reactively-loaded non-periodic slow-wave artificial transmission lines for stop band bandwidth enhancement: Application to power splitters. *Int J Microwave Wireless Techn*. 2019;11(5-6):475-481.

[14] Kianinejad A, Chen ZN, Qiu C. Full modeling, loss reduction, and mutual coupling control of spoof surface plasmon-based meander slow wave transmission lines. *IEEE Trans Microwave Theory Techn*. 2018;66(8):3764-3772.

[15] Qian ZY, Chen JX. Compact bandpass filter using CMRC-based dual-behavior resonator. *Int J RF Microw Comput Aided Eng*. 2019;29:e21719.

[16] Chen S, Guo M, Xu K, Zhao P, Dong L, Wang G. A frequency synthesizer based microwave permittivity sensor using CMRC structure. *IEEE Access*. 2018;6:8556-8563.

[17] Wang D, Chin K, Che W, Wu Y, Chang C. Compact 60 GHz low-temperature cofired ceramic filter with quasi-elliptic bandpass response. *IET Microw Ant Propag*. 2016;10(6):664-669.

[18] Joseph N, Varghese J, Teirikangas M, Vahera T, Jantunen H. Ultra-low-temperature cofired ceramic substrates with low residual carbon for next-generation microwave applications. *ACS Applied Materials Interfaces*. 2019;11(26):23798-23807.

[19] Torun HM, Swaminathan M. High-dimensional global optimization method for high-frequency electronic design. *IEEE Trans Microwave Theory Techn*. 2019;67(6):2128-2142.

[20] Wang D, Hu Y, Yue W, Zeng Y, Tu Z, Cai Y, Wang W, Fang Q, Yu M. Broadband and compact polarization beam splitter based on an asymmetrical directional coupler with extra optimizing designs. *Appl Opt*. 2019;58:8221-8226.

[21] Zhang W, Feng F, Gongal-Reddy VWR, Zhang J, Yan S, Ma, Zhang QJ. Space mapping approach to electromagnetic centric multiphysics parametric modeling of microwave components. *IEEE Trans Microwave Theory Techn*. 2018;66(7):3169-3185.

[22] Koziel S, Leifsson L. *Simulation-driven design by knowledge-based response correction techniques*. Springer, Cham; 2016.

[23] Koziel S, Bekasiewicz A. Fast simulation-driven feature-based design optimization of compact dual-band microstrip branch-line coupler. *Int J RF Microwave CAE*. 2015;26(1):13-20.

[24] Feng F, Zhang C, Na W, Zhang J, Zhang W, Zhang QJ. Adaptive feature zero assisted surrogate-based EM optimization for microwave filter design. *IEEE Microw Wireless Compon Lett*. 2019;29(1):2-4.

[25] Feng F, Zhang C, Zhang S, Gongal-Reddy VMR, Zhang QJ. Parallel EM optimization approach to microwave filter design using feature assisted neuro-transfer functions. *IEEE MTT-S Int Microw Symp Dig*, San Francisco, CA, 2016:1-3.

[26] Malhi H, Bakr MH. Geometry evolution of microwave filters exploiting self-adjoint sensitivity analysis. *Int. Conf. Numerical Electromagn Multiphysics Mod Opt (NEMO)*, Ottawa, Canada, 2015.

[27] Koziel S, Bekasiewicz A. Point-by-point Pareto front exploration and adjoint sensitivities for rapid multi-objective optimization of compact impedance matching transformers. *Int J Numer Model*. 2018;31(5):e2350.

[28] Joung J. Machine learning-based antenna selection in wireless communications. *IEEE Comm Lett*. 2016;20(11):2241-2244.

[29] Xiao L, Shao W, Ding X, Wang B. Dynamic adjustment kernel extreme learning machine for microwave component design. *IEEE Trans Microwave Theory Techn*. 2018;66(10):4452-4461.

[30] Koziel S, Bekasiewicz A. *Multi-objective design of antennas using surrogate models*. World Scientific, Singapore; 2016.

[31] Yilmaz T, Hasan N, Zane R, Pantic Z. Multi-objective optimization of circular magnetic couplers for wireless power transfer applications. *IEEE Trans Magn*. 2017;53(8):1-12.

[32] Dong J, Li Q, Deng L, Fast multi-objective optimization of multi-parameter antenna structures based on improved MOEA/D with surrogate-assisted model, *AEU Int J Electr Com*m; 2017;72:192-199.

[33] Koziel S, Bekasiewicz A. Strategies for computationally feasible multi-objective simulation-driven design of compact RF/microwave components. *Eng Comput*. 2016;33(1):184-201.

[34] Markley L, Eleftheriades GV. An ultra-compact microstrip crossover inspired by contra-directional even and odd mode propagation. *IEEE Microwave Wireless Comp Lett*. 2014;24(7):436-438.

[35] Pietrenko-Dabrowska A, Koziel S. Numerically efficient algorithm for compact microwave device optimization with flexible sensitivity updating scheme. *Int J RF Microw Comput Aided Eng*. 2019;29(7):e21714.

[36] Nocedal J, Wright SJ. *Numerical optimization*. Springer Series in Operations Research, Springer; 2000.

[37] Jin N, Rahmat-Samii Y. Advances in particle swarm optimization for antenna designs: realnumber, binary, single-objective and multiobjective implementations. *IEEE Trans Ant Prop.* 2007;55(3):556-567.

[38] Feliot P, Bect J, Vazquez E. A Bayesian approach to constrained single- and multi-objective optimization. *J Global Opt*. 2017;67(1):1-37.

[39] Koziel S, Bekasiewicz A, Zieniutycz W. Expedited EM-driven multi-objective antenna design in highly-dimensional parameter spaces. *IEEE Ant Wireless Prop Lett*. 2014;13:631-634.

[40] Rao SS. *Engineering Optimization*: *Theory and Practice*. John Wiley & Sons; 2009.

[41] Koziel S, Bekasiewicz A. Fast EM-driven size reduction of antennastructures by means of adjoint sensitivities and trust regions. *IEEE Ant Wireless Prop Lett*. 2015;14:1681-1684.

[42] Johanesson DO, Koziel S, Bekasiewicz A. EM-driven constrained miniaturization of antennas using adaptive in-band reflection acceptance threshold. *Int J Numer Model*. 2019;32(2):e2513.

[43] Deb K. *Multi-objective optimization using evolutionary algorithms*. Wiley, New York; 2001

[44] Lalbakhsh A, Afzal MU, Esselle KP, Zeb BA. Multi-objective particle swarm optimization for the realization of a low profile bandpass frequency selective surface. *2015 Int Symp Antennas Propagation (ISAP)*. Hobart, TAS, 2015;1-4.

[45] Zheng LM, Zhang SX, Zheng SY, Pan YM. Differential evolution algorithm with two-step subpopulation strategy and its application in microwave circuit designs. *IEEE Trans Industrial Inf*. 2016;12(3):911-923.

[46] Baumgartner P, Bauernfeind T, Bíró O, Hackl A, Magele C, Renhart W, Torchio R. Multi-objective optimization of Yagi–Uda antenna applying enhanced firefly algorithm with adaptive cost function. *IEEE Trans Magn*. 2018;54(3):1-4.

[47] Liu Y, Cheng QS, Koziel S. A generalized SDP multi-objective optimization method for EM-based microwave device design. *Sensors*, 2019;19:3065.

[48] Nedjah N, Mourelle LM. Evolutionary multi-objective optimisation: a survey. *Int J Bio-Inspir Comput*. 2015;7(1)1-25.

[49] Long Q, Wu C, Huang T, Wang X. A genetic algorithm for unconstrained multi-objective optimization. *Swarm Evolut Comput*. 2015;22:1-14.

[50] Koziel S, Pietrenko-Dabrowska A. Performance-based nested surrogate modeling of antenna input characteristics. *IEEE Trans Ant Prop*. 2019;67(5):2904-2912.

[51] Goudos SK, Diamantoulakis PD, Karagiannidis GK. Multi-objective optimization in 5G wireless networks with massive MIMO. *IEEE Comm Lett*. 2018;22(11):2346-2349.

[52] Wang L, Wang G, Sidén J. Design of high-directivity wideband microstrip directional coupler with fragment-type structure. *IEEE Trans Microwave Theory Techn*. 2015;63(12):3962-3970.

[53] Zheng SY, Zhang SX. A jumping genes inspired multi-objective differential evolution algorithm for microwave components optimization problems, *Applied Soft Computing*. 2017;59:276-287.

[54] Koziel S, Bekasiewicz A, Kurgan P, Bandler JW. Rapid multi-objective design optimisation of compact microwave couplers by means of physics-based surrogates. *IET Microw Ant Propag*. 2016;10(5):479-486.

[55] Koziel S, Bekasiewicz A, Kurgan P. Rapid multi-objective simulation-driven design of compact microwave circuits. *IEEE Microwave Wireless Comp Lett*. 2015;25(5):277-279.

[56] Koziel, S, Bekasiewicz, A, Szczepanski, S. Multi-objective design optimization of antennas for reflection, size, and gain variability using kriging surrogates and generalized domain segmentation. *Int J RF Microw Comput Aided Eng*. 2018;28(5):e21253.

[57] Couckuyt I, Declercq F, Dhaene T, Rogier H, Knockaert L. Surrogate-based infill optimization applied to electromagnetic problems. *Int J RF and Microwave Comp Aid Eng*, 2010;20(5):492-501.

[58] Dong J, Qin W, Wang M. Fast multi-objective optimization of multi-parameter antenna structures based on improved BPNN surrogate model. *IEEE Access*. 2019;7:77692-77701.

[59] Acampora G, Herrera F, Tortora G, Vitiello A. A multi-objective evolutionary approach to training set selection for support vector machine. *Knowledge-Based Syst.* 2018;147:94-108.

[60] Kurgan P, Koziel S. Surrogate-assisted multi-objective optimization of compact microwave couplers. *J Electromagn Waves App*. 2016;30(15):2067-2075.

[61] Martínez SZ, Coello CAC. Combining surrogate models and local search for dealing with expensive multi-objective optimization problems. *2013 IEEE Congress Evol Comput*. Cancun, 2013:2572-2579.

[62] Coello Coello CA. *Evolutionary algorithms for solving multi-objective problems*. Springer; 2007.

[63] Feng F, Zhang J, Zhang W, Zhao Z, Jin J, Zhang Q. Coarse- and fine-mesh space mapping for EM optimization incorporating mesh deformation. *IEEE Microwave Wireless Comp Lett*. 2019;29(8):510-512.

[64] Koziel S, Ogurtsov S. Multi-objective design of antennas using variable-fidelity simulations and surrogate models. *IEEE Trans Ant Propag*. 2013;61(12):5931-5939.

[65] Koziel S, Bekasiewicz A. Rapid multiobjective antenna design using point-by-point Pareto set identification and local surrogate models. *IEEE Trans Antennas Propag*. 2016;64(6):2551-2556.

[66] Koziel S, Bekasiewicz A. Rotational design space reduction for cost-efficient multi-objective antenna optimization. *Europ Conf Ant Prop*, Lisbon, Portugal, 2015:1-4.

[67] Koziel S, Sigurdsson AT. Triangulation-based constrained surrogate modeling of antennas. *IEEE Trans Ant Propag*. 2017;66(8):4170-4179.

[68] Simpson TW, Pelplinski JD, Koch PN, Allen JK. Metamodels for computer-based engineering design: survey and recommendations. *Eng Computers*. 2001;17:129-150.

[69] Koziel S, Bekasiewicz A. Rapid simulation-driven multi-objective design optimization of decomposable compact microwave passives. *IEEE Trans Microwave Theory Techn*. 2016;64:2454-2461.